Electronic Supplementary Material (ESI) for Nanoscale.
This journal is © The Royal Society of Chemistry 2015

Supplementary Information for

Enhanced in-plane thermoelectric figure-of-merit in p-type SiGe thin films by nanograin boundaries

Jianbiao Lu, Ruiqiang Guo, Weijing Dai and Baoling Huang[a)]
Department of Mechanical and Aerospace Engineering, The Hong Kong University of Science and Technology, Clear Water Bay, Kowloon, Hong Kong

In-plane thermal conductivity fitting from the 2 line 3ω method

The samples used contain 4 layers (50nm ALD, 1μm SiGe, 1μm SiO_2 and 400μm Si from top down. The anisotropic thermal transport properties are measured based on a general two-dimensional heat-conduction model across the multilayer system and a uniform heat flux boundary condition between the heater and the top film. The complex temperature rise of a heater is [1,2]

$$\Delta T = \frac{-p}{\pi l k_{y1}} \int_0^\infty \frac{1}{A_1 B_1} \frac{\sin^2(\mathrm{b}\lambda)}{b^2 \lambda^2} d\lambda \,, \qquad \text{(S1)}$$

where

$$A_{i-1} = \frac{A_i \frac{k_{y_i} B_i}{k_{y_{i-1}} B_{i-1}} - \tanh(\varphi_{i-1})}{1 - A_i \frac{k_{y_i} B_i}{k_{y_{i-1}} B_{i-1}} \tanh(\varphi_{i-1})}, i = 2...n \, , \; B_i = \left(k_{xyi} \lambda^2 + \frac{i2\omega}{\alpha_{yi}} \right)^{1/2} ,$$

$$\varphi_i = B_i d_i , \qquad k_{ky} = k_x / k_y .$$

Here n is the total number of layers including the substrate, subscript i labels the ith layer starting from the top, subscripts x and y correspond to the in-plane and cross-plane directions respectively, b is the heater half width, k is the thermal conductivity of the layer, ϖ is the angular modulation frequency of the current, d is the layer thickness, and α is the thermal diffusivity. The anisotropy of the thermal conductivity is introduced through the term k_{xy} , the ratio of the in-plane to cross-plane thermal conductivity of the layer.

The fitting is basically a three-step process. Firstly the sample and a reference with wide heater lines are used to independently determine the cross-plane thermal conductivity. Secondly the sample with a heater line with a linewidth comparable to the targeted layer thickness is used to obtain signals containing the anisotropic thermal property information. Thirdly, the in-plane thermal conductivity of the targeted SiGe layer is fitted to the experimental data according to the temperature rise of the line heater under different frequencies (Eq. S1).

Heat loss analysis in 3ω measurement

The two heater lines will work individually with no interaction with each other. Heat loss from the top surface of the 3ω patterns will be estimated in the case of a sample being measured in the vacuum chamber with the pressure better than 10^{-5} Torr at 300 K. During the measurement, the

heater line will be heated up. Here two factors are taken into consideration: radiation to the chamber shield and conduction heat loss by the residual air in the chamber.

The radiation is estimated from:

$$Q_{rad} = \varepsilon \sigma A (T_m^4 - T_0^4) \qquad \text{* MERGEFORMAT S.1}$$

where ε is the emissivity of the heater line, σ is the Stefan–Boltzmann constant, A is the effective surface area of the heater line. T_m and T_0 are the temperatures of the heater line and the radiation shield of the chamber, respectively. The upper bound of $\varepsilon = 1$ is chosen. A is 20×700 μm^2 for the wide heater line and 2×70 μm^2 for the thin one. T_m-T_0 is less than 1 K and less than 10 K for the wide and thin heater line, respectively, which agrees with other reported work[2, 3]. Thus, the Q_{rad} can be readily calculated to be 8.6×10^{-8} W and 9.0×10^{-9} W for the wide and thin heater lines, respectively, which is negligibly small compared to the heating power (~10 mW in both cases).

The heat loss by the residual air:

$$Q_{air} = G_{air}(T_m - T_0) \qquad \text{* MERGEFORMAT S.2}$$

where $G_{air} = k_{air} A / D$ is the thermal conductance of the residual air, and D is the distance from the sample to the radiation shield. The MFP of the air molecules at such a pressure is of the order of 10m, much larger than D, so $G_{air} = \frac{1}{3} C_{air,vac} A v$, $C_{air,vac}$ and v are the specific heat capacity of the residual air at constant volume and velocity of air molecules. $C_{air,vac}$ is of the order 10^{-4} J/(m^3-K) at 10^{-5} Torr and v can be estimated to be 660 m/s for diatomic gas (eg. N_2) case. So that Q_{air}

can be estimated to be 3×10^{-10} and 3×10^{-11} for wide and thin line cases, respectively. Still the values are too small to affect our measurement accuracy.

Determining fitting parameters for bulk Si, Ge and SiGe alloy

The temperature-dependent lattice thermal conductivity of the polycrystalline SiGe layer can be modelled with a Callaway-form approximate analytic solution to Boltzmann Transport Equations for phonons[4-6], which assumes a linear dispersion for acoustic phonons and neglects the contributions from optical phonons, i.e.,

$$\kappa = \left(\frac{k_B T}{\hbar}\right)^3 \frac{k_B}{2\upsilon\pi^2} \int_0^{\hbar\omega_c/k_B T} \tau(T,y) y^4 \frac{\exp(y)}{[\exp(y)-1]^2} dy , \qquad \text{* MERGEFORMAT S.3}$$

where k_B is Boltzmann constant, T is temperature, $\hbar$ is the reduced Plank's constant, υ is the acoustic phonon group velocity and $y = \hbar\omega/k_B T$ is the dimensionless phonon angular frequency. The phonon group velocity υ of $Si_{(1-x)}Ge_x$ alloy is calculated by $\upsilon = [(1-x)\upsilon_{Si}^{-2} + x\upsilon_{Ge}^{-2}]^{-1/2}$, where x is the Ge concentration and $\upsilon_{\mathrm{Si\,(Ge)}} = (1/3\upsilon_{\mathrm{Si\,(Ge),\,L}}^{-2} + 2/3\upsilon_{\mathrm{Si\,(Ge),\,T}}^{-2})^{-1/2}$ (L and T denote longitudinal and transversal acoustic group velocities, respectively) are the average sound speeds for Si (6400 m/s) and Ge (3900 m/s) from experiments, respectively[5]. The cutoff frequency ω_c is obtained by $\omega_c = 2\pi\upsilon/a$, where the lattice constant a is approximated by $a = (1-x)a_{Si} + xa_{Ge}$ according to Vegard's law[6]. The total scattering rate for bulk SiGe alloy is calculated by considering Umklapp phonon-phonon scattering and alloy scattering according to Matthiessen's rule,

$$\tau^{-1} = \tau_U^{-1} + \tau_{alloy}^{-1} . \qquad \text{* MERGEFORMAT S.4}$$

Based on the virtual crystal approximation, the Umklapp scattering rate is expressed as,

$$\tau_U^{-1} = (1-x)\tau_{U,Si}^{-1} + x\tau_{U,Ge}^{-1},$$ * MERGEFORMAT S.5

with $\tau_{U,Si(Ge)}^{-1} = B_{Si(Ge)}\exp(-C_{Si(Ge)}/T)\omega^2 T$. The alloy scattering term is defined as $\tau_{alloy}^{-1} = x(1-x)A\omega^4$.

Figure S1 shows the temperature dependence of modeling results for bulk Si and Ge, agreeing well with the experimental results[7, 8].

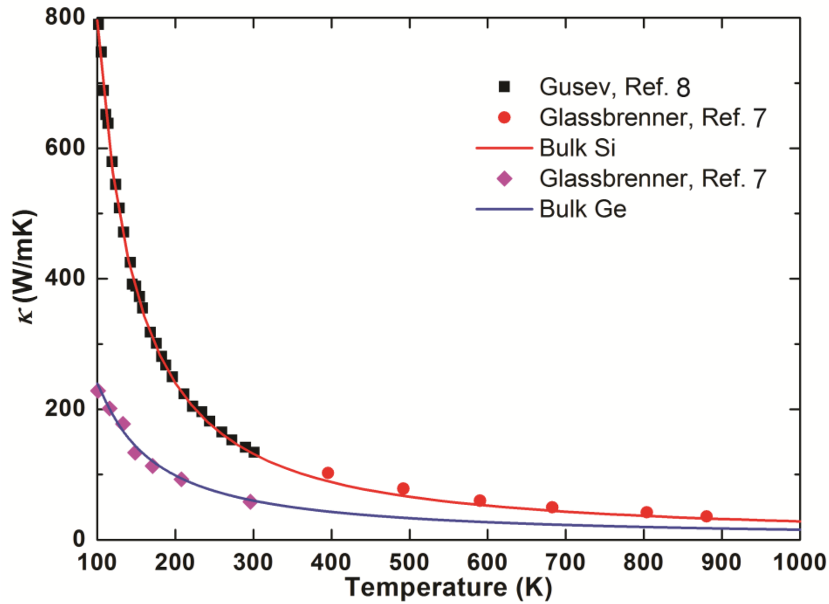

Figure S1. Temperature dependence of modeling (lines) and experimental (dots) lattice thermal conductivities of bulk Si and Ge from 100 K to 1000 K.

Based on the fitting parameters for bulk Si and Ge, we further modeled the lattice thermal conductivity of bulk SiGe alloy as a function of the Ge concentration at room temperature, as shown in Fig. S2. One can find reasonable agreements between the modeling results and experimental values[9, 10]. By making comparison with the ab initio results[11], we find that the virtual crystal method significantly overestimates the thermal conductivity contribution of phonon modes near the Gamma point. This is caused by the overestimated relaxation time near

the Gamma point, which has been highlighted in a previous ab initio investigation[11]. Thus, we propose to remove the contribution of phonon modes with frequency less than 0.1 THz, which is negligible according to the ab initio calculations[11]. For the modeling of bulk Si and Ge, such a treatment is not necessary.

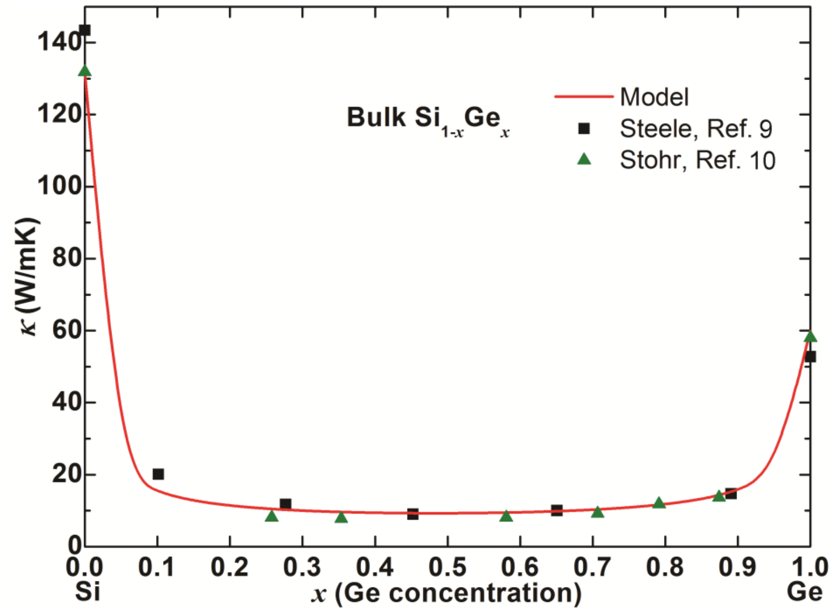

Figure S2. Modeling (line) and experimental (dots) lattice thermal conductivities of bulk $Si_{1-x}Ge_x$ alloy as a function of the Ge concentration x at room temperature.

References

1 J. P. Feser, Ph.D. thesis, University of California, Berkeley, 2010.
2 T. Borca-Tasciuc, A. R. Kumar and G. Chen, *Rev. Sci. Instrum.*, 2001, **72**, 2139.
3 Y. Ju, K. Kurabayashi and K. Goodson, *Thin Solid Films*, 1999, **339**, 160-164.
4 J. Callaway, *Phys. Rev.*, 1959, **113**, 1046-1051.
5 Z. Wang and N. Mingo, *Appl. Phys. Lett.*, 2010, **97**, 101903.
6 R. Cheaito, J. Duda, T. Beechem, K. Hattar, J. Ihlefeld, D. Medlin, M. Rodriguez, M. Campion, E. Piekos and P. Hopkins, *Phys. Rev. Lett.*, 2012, **109**, 195901.
7 C. Glassbrenner and G. Slack, *Phys. Rev.*, 1964, **134**, A1058-A1069.
8 A. V. Gusev, A. M. Gibin, O. N. Morozkin, V. A. Gavva and A. V. Mitin, *Inorg. Mater.*, 2002, **38**, 1100-1102.
9 M. C. Steele and F. D. Rosi, *J. Appl. Phys.*, 1958, **29**, 1517.

10 H. Stohr and W. Klemm, *Z. Anorg. Allg. Chem.*, 1954, **241**, 304.
11 J. Garg, N. Bonini, B. Kozinsky and N. Marzari, *Phys. Rev. Lett.*, 2011, **106**, 045901.